ARTICLE

Investigation of recrystallization behavior of large sized Nb–V microalloyed steel rod during thermomechanical controlled processing

Wenfei Shen, Chi Zhang, Liwen Zhang,[a) and Qianhong Xu
School of Materials Science and Engineering, Dalian University of Technology, Dalian 116023, China

Yifeng Xu and Lifang Bie
Suxin Special Steel Group Co., Ltd., Suzhou 215151, China

To investigate the recrystallization behavior of large sized Nb–V microalloyed steel rods during thermomechanical controlled processing (TMCP), a series of isothermal hot compression tests were conducted on a Gleeble 1500 thermomechanical simulator. The kinetics and microstructure evolution models of dynamic recrystallization, static recrystallization, metadynamic recrystallization and the grain growth model of the tested steel were developed. Based on the developed models, a finite element (FE) model coupled with the recrystallization behavior of large sized Nb–V microalloyed steel rods during TMCP was established. Then, the distributions and evolutions of recrystallization fraction and grain size during the whole deformation process are obtained and analyzed. Finally, the predicted results were compared with experimental ones, and they show good agreement. This illustrates that the recrystallization models of the tested steel are valid and the developed FE model of large sized Nb–V microalloyed steel rods during TMCP is effective.

I. INTRODUCTION

Nb–V microalloyed nonquenched and tempered steel is widely used in industry. This steel can be directly used for cutting after hot rolling without heat treatment and straightening operations because the mechanical properties can be obtained at the end of hot forming process. Therefore, much money and energy can be saved, and it is drawing more and more attention from society.[1–4]

However, the properties of the steel rod need further improvement, especially for the large sized steel rod. This is because the properties of the steel rod decrease with increasing of the rod size. This phenomenon is largely determined by the uniform distribution of microstructures.[5,6] And the previous researches indicate that the microstructure evolution in a rod piece during hot deformation is complex and it is affected by dynamic recrystallization (DRX), metadynamic recrystallization (MDRX), static recrystallization (SRX), and grain growth.[7–11] And these microstructure evolution behaviors are as well influenced by the macroscopic factors such as deformation temperature, strain, and strain rate.[12–17] Therefore, it is necessary to clearly understand the recrystallization behaviors and the microstructure evolution during hot deformation and provide guidance for designing optimal processing of large sized Nb–V microalloyed steel rods.

Recently, with the development of numerical simulation technology, many researchers have used the finite element method (FEM) to predict the microstructure evolution during the hot deformation process for various metal materials. Li et al.[18] built a coupling multivariable simulation model for hot strip continuous rolling. The evolution laws of strain, temperature, and microstructure were analyzed. Chen et al.[19] simulated the hot forging process of turbine blades for martensitic stainless steel. Yue et al.[20] investigated the 18-pass hot rolling process of a GCr15 steel rod using a multifield coupled FE model. And the evolution of the recrystallization behavior and austenite grain size is predicted. Jiang et al.[21] studied the microstructure evolution of alloy 690 during the hot extrusion process. The simulated microstructure agrees well with the actual one. There are also some other researches about the microstructure simulation.[22–29] These researches confirm that the FEM is a reliable approach to investigate microstructure evolution during the rod rolling process.

In this paper, a series of isothermal hot compression tests were conducted. Then, the mathematic models for DRX, SRX, MDRX, and grain growth were developed. Based on the mathematic models, a multifield FE model coupled with the microstructure prediction of large sized Nb–V microalloyed steel rods during thermomechanical controlled processing (TMCP) was established.

The evolutions of recrystallization and austenite grain size during the whole deformation process were simulated. Finally, comparisons between the simulated results and experimental ones were carried out.

II. EXPERIMENTAL PROCEDURE

The chemical compositions of the tested steel in this paper are given in Table I. The DRX, MDRX, SRX, and grain growth behaviors are investigated by isothermal hot compression tests using a Gleeble 1500 thermomechanical simulator (Dynamic Systems Inc., Poestenkill, New York). The specimen for tests is a cylinder with a diameter of 8 mm and height of 12 mm.

A. DRX tests

In DRX tests, a single pass isothermal hot compression is applied. The specimens were heated to 1523 K at the rate of 20 K/s and held for 300 s. Then, a wide range of temperatures (1123–1473 K) and strain rates (0.01–10 s^{-1}), deformation conditions, are carried out to a true strain of 0.8. After compression, all specimens are water quenched to room temperature immediately. Finally, the specimens are sectioned along the axial direction and the sections of the specimens were polished and etched. The microstructures in the sections were examined by an optical microscope.

B. MDRX tests

In MDRX tests, a double passes isothermal hot compression is applied. The specimens were heated to 1473 K at the rate of 20 K/s and held for different times (3–9 min). Then, the first compressions were conducted with a strain of 0.4 at a wide range of temperatures (1273–1423 K) and strain rates (0.01–5 s^{-1}). After different interpass times (0.5–10 s), the second compression with a strain of 0.1 was conducted at the same condition. After compression, the same operations with DRX specimens were conducted.

C. SRX tests

In SRX tests, a double pass isothermal hot compression is also applied. The specimens were heated to 1473 K at the rate of 20 K/s and held for different times (0–3 min). Then, the first compressions were conducted with a prestrain of 0.15–0.25 at a wide range of temperatures (1123–1423 K) and strain rates (0.01–5 s^{-1}). After different interpass times (0.5–30 s), the second compression with a strain of 0.1 was conducted at the same condition. After compression, the same operations with DRX specimens were conducted.

TABLE I. Chemical compositions of the tested steel (wt%).

C	Si	Mn	P	S	Cr	V	Nb
0.38–0.45	0.45	1.50	≤0.02	≤0.04	0.25	0.05	0.02

D. Grain growth tests

The grain growth experiment is performed at the holding temperature of 1273–1523 K and holding time of 0–180 s. Then, the specimens are water quenched to room temperature immediately. The microstructures in the section of the specimen are examined by an optical microscope.

III. RECRYSTALLIZATION MODEL AND GRAIN GROWTH MODEL

The typical experimental curves obtained from the tests are showed in Fig. 1. It can be seen from Fig. 1(a) that the curves under high temperatures (1273–1423 K) exhibit typical a DRX behavior, but the other curves show a dynamic recovery character. This is because DRX is a thermally activated process. With the increase in temperature, the formation of DRX nuclei becomes easier, and meanwhile, the grain boundary mobility increases, resulting in increasing of the rate of DRX. Figure 1(b) shows the stress–strain curves of MDRX tests. It can be seen that the strain in the first compression is larger than the peak strain, which indicates that a certain amount of DRX has occurred during the first compression. The stress in the second compression decreases with increasing of interpass time, indicating that the softening fraction of MDRX increases with increasing of interpass time. It can be found that from the stress–strain curves of SRX tests, as shown in Fig. 1(c), the strain in the first compression is much smaller than the peak strain, which indicates that no DRX has occurred. The stress in the second compression decreases with increasing of interpass time before 10 s, and the others are approximate after 10 s. It illustrates that the softening fraction of SRX increases with increasing of interpass time and it reaches maximum at 10 s.

According to the obtained flow stress curves and the microstructures in the sections of the specimens, the kinetics and grain size model of DRX, MDRX and SRX and the grain growth model of the tested steel were established using the previous methods.[30–33] The DRX model is shown below,

$$\text{DRX model} \begin{cases} Z = \dot{\varepsilon} \exp\left(\frac{318.7 \times 10^3}{RT}\right) \\ \varepsilon_c = 2.997 \times 10^{-3} Z^{0.164} \\ X_{DRX} = 1 - \exp\left[-0.693\left(\frac{t_d}{t_{0.5/DRX}}\right)^{2.013}\right] \\ t_{0.5/DRX} = 2.566 \times 10^{-2} \dot{\varepsilon}^{-0.857} \exp\left(\frac{29315.62}{RT}\right) \\ D_{DRX} = 12751.222 \cdot Z^{-0.211} \end{cases},$$

(1)

where $\dot{\varepsilon}$ is the strain rate, R is the universal gas constant, T is the absolute temperature, ε_c is the critical strain, X_{DRX} is the fraction of DRX, t_d is the deformation time after critical strain, $t_{0.5/DRX}$ is the time for 50% fraction of DRX, D_{DRX} is the grain size after DRX.
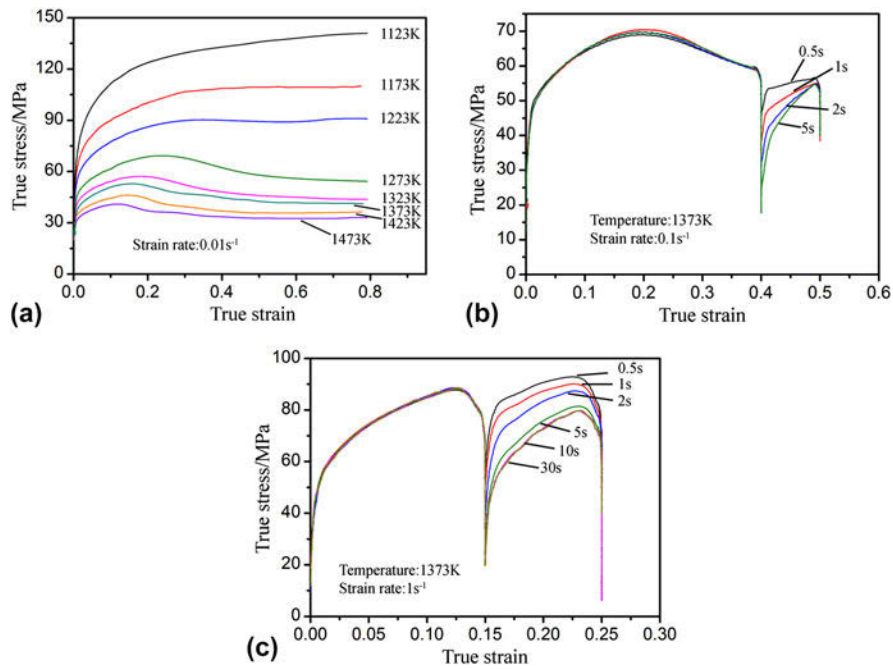
FIG. 1. Typical flow stress curves of (a) DRX; (b) MDRX; (c) SRX.

The obtained MDRX model is shown as follows:

$$\text{MDRX model}\begin{cases} X_{\text{MDRX}} = 1 - \exp\left(-0.693\left(\frac{t_{\text{m}}}{t_{0.5/\text{MDRX}}}\right)^{1.113}\right) \\ t_{0.5/\text{MDRX}} = 1.697 \times 10^{-6}\dot{\varepsilon}^{-0.378} d_0^{0.227} \exp\left(\frac{127366}{RT}\right) \\ D_{\text{MDRX}} = 1804.58\dot{\varepsilon}^{-0.117} d_0^{0.63} \exp\left(\frac{-73778.4}{RT}\right) \end{cases},$$

(2)

where X_{MDRX} is the volume fraction of MDRX and its value is assumed to be the same as the MDRX softening fraction, t_{m} is the interpass time, $t_{0.5/\text{MDRX}}$ is the time for 50% fraction of MDRX, d_0 is the initial grain size, D_{MDRX} is the grain size after MDRX.

The established SRX model is shown as follows:

$$\text{SRX model}\begin{cases} F_{\text{SRX}} = 1 - \exp\left(-0.693\left(\frac{t_{\text{s}}}{t_{0.5/\text{SRX}}}\right)^{f(T)}\right) \\ f(T) = 0.00372T - 3.9944 \\ t_{0.5/\text{SRX}} = 3.363 \times 10^{-10}\varepsilon^{-1.683}\dot{\varepsilon}^{-0.385} d_0^{0.642} \exp\left(\frac{183520.8}{RT}\right) \\ X_{\text{SRX}} = \frac{F_{\text{SRX}}-0.2}{1-0.2} \\ D_{\text{SRX}} = 67.42\varepsilon^{-0.627}\dot{\varepsilon}^{-0.136} d_0^{0.281} \exp\left(\frac{-28025.7}{RT}\right) \end{cases},$$

(3)

where F_{SRX} is the softening fraction of SRX, t_{s} is the interpass time, $t_{0.5/\text{SRX}}$ is the time for 50% softening fraction of SRX, X_{SRX} is the SRX fraction, D_{SRX} is the grain size after SRX.

The grain growth model for the tested steel can be described as follows:

$$D^7 = D_0^7 + 1.54 \times 10^{39} t \exp\left(\frac{-768821}{RT}\right), \quad (4)$$

where D is the austenite grain size at time t and D_0 is the initial grain size.

IV. RECRYSTALLIZATION BEHAVIOR DURING TMCP

A. Integration of mathematic models

To carry out the multifield coupled hot rolling process of Nb–V microalloyed nonquenched and tempered steel bars, an MSC.Marc subprogram was designed to predict the evolution of the recrystallization behavior and austenite grain size. The flowchart of the subprogram is shown in Fig. 2. The whole rolling process can be divided into two parts. One is rolling and in the first step of rolling period, the recrystallization fraction is returned to zero. Then, the strain will be compared to the critical strain of DRX. If the strain is larger than the critical strain, DRX will take place or the strain will continue to accumulate. The other one is interpass and during this period if the recrystallization fraction is larger than 0.95, the grain growth will be calculated. Otherwise, MDRX will occur if DRX is larger than 0.05, or SRX will occur if DRX is smaller than 0.05. Then the subprogram will continue step by step till the whole process is over. In the grain size calculation, the initial grain size is assumed to be 200 μm. This is because the effect of different initial grain sizes will disappear after several sufficient cycles of recrystallization during multipass continuous rolling.[29,34,35] Then, the average grain size is calculated according to the following equations:
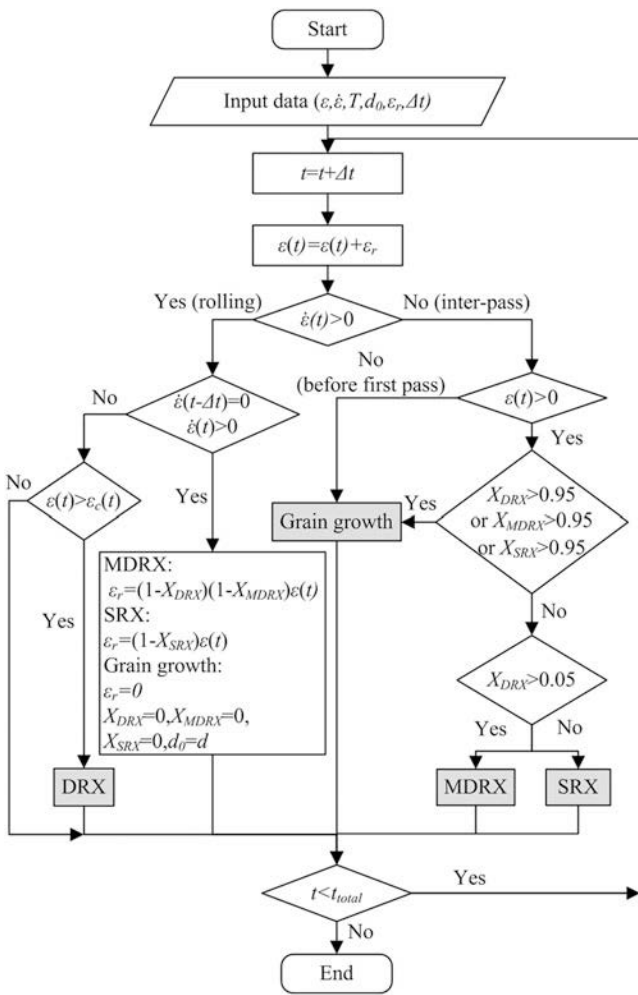
FIG. 2. Flowchart of the subprogram for microstructure evolution.

$$\text{DRX} : d = X_{\text{DRX}}d_{\text{DRX}} + (1 - X_{\text{DRX}})d_0 \quad , \quad (5)$$

$$\text{SRX} : d = X_{\text{SRX}}d_{\text{SRX}} + (1 - X_{\text{SRX}})d_0 \quad , \quad (6)$$

$$\text{MDRX} : d = X_{\text{DRX}}d_{\text{DRX}} + (1 - X_{\text{DRX}})X_{\text{MDRX}}d_{\text{MDRX}}$$
$$+ (1 - X_{\text{DRX}})(1 - X_{\text{MDRX}})d_0 \quad . \quad (7)$$

B. FE model

The layout of rolling mills for rod rolling of Nb–V microalloyed nonquenched and tempered steel bars is shown in Fig. 3(a). It can be seen that there are roughing mill, intermediate mill, and finishing mill in the production line. The roughing and intermediate mills are reversing mills and finishing mill is a one-way rolling mill. The Nb–V microalloyed nonquenched and tempered steel is rolled from a square billet of 220×220 mm to a rod of

$\phi90$ mm. The rolling process consists of 8 roughing passes, 3 intermediate passes, and 1 finishing pass. Considering the consistence of the microstructure and mechanical properties of rods at the rolling direction in the steady rolling region, only 600 mm length of billet is used. Due to the symmetry, a quarter of a billet and roller is included. The FE model for descaling and the first 2 passes in roughing rolling are shown in Fig. 3(b). In the model, the rollers are individually driven with an alternate vertical and horizontal arrangement. When one pass is finished, the corresponding roller will be removed and the next roller will be arranged into the production line. Two pushing rigid bodies are used to push the billet into the roller as the function of the conveyer. When the first model is finished, all physical field data will be transferred into the next model by a data transfer technique.[36,37] The subprogram developed above is coupled with the FE model to analyse the recrystallization behavior during the rod rolling process.

C. Simulation results and discussion

1. Field-variables distribution

The field-variables such as temperature, strain, and strain rate during the rolling process have a significant influence on the microstructure evolution. Therefore, it is important to clarify the distribution of field-variables during the rolling process. The temperature distribution in the rolled piece, for example, at the 6th pass, is shown in Fig. 4(a). It can be seen that the closer to the center, the higher the temperature. And the lowest temperature appeared at the surface in touch with the roller. It can be easily found from Fig. 4(b) that the distribution of the effective strain is inhomogeneous. This may induce the inhomogeneous distribution of recrystallization because of its great effect on the recrystallization behavior. From Fig. 4(c), it is obvious that during the steady rolling stage, the larger strain rate appears at the subsurface of the rod piece. But it is small at the surface in touch with the roller because of the effect of the undeformed zone.

2. Recrystallization behavior

Figure 5 shows the typical distribution of recrystallization fraction during roughing rolling (e.g., 4th pass), intermediate rolling (e.g., 9th pass), and finishing rolling (12th pass). It can be seen that a certain amount of DRX has occurred in most of the central part of the rolled piece due to the high temperature and large reduction during the roughing rolling process. And the area near the surface has no DRX for the small strain. Then, during the interpass time, MDRX takes place in the area where DRX has occurred, and SRX takes place in the other area. During the intermediate
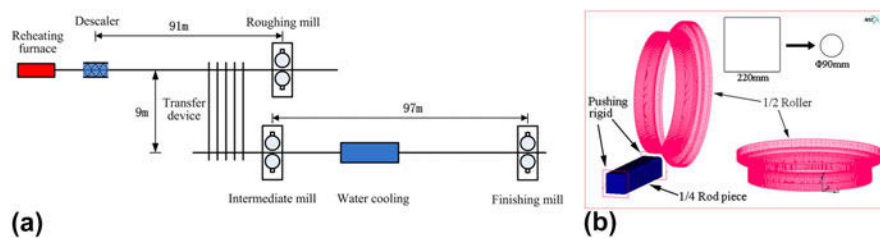
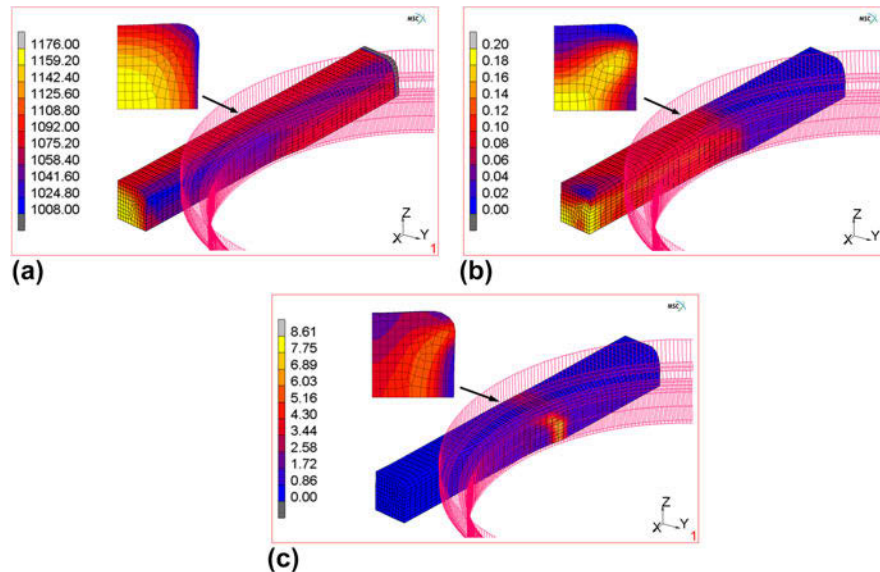FIG. 3. (a) Schematic representation of the rolling process and (b) the corresponding FE model.

FIG. 4. Field-variable distributions in the rolled piece at the sixth pass (a) temperature; (b) effective strain; (c) effective strain rate.

rolling process, only some amount of DRX occurred in a small area of the central part of the rolled piece. This is because the deformation of the rod decreases with decreasing section area. From Fig. 5, it can be found that no DRX occurred during the finishing rolling process and only some amount of SRX takes place during the interpass time. This phenomenon is attributed to the low temperature and small reduction of the rolled piece during the finishing rolling process. Figure 6 shows the evolution of recrystallization fractions at the center of the rolled piece. It can be seen that the DRX fraction is relatively small during the whole rolling process, and SRX and MDRX are the main methods to refine the microstructure. This is because the size of the rod is large, and the strain in the center of the rod is hard to reach the critical strain or completely finish DRX, so the DRX fraction is relatively small.

The evolution of the average grain size at different positions during the whole rolling process is shown in Fig. 7. It can be seen from the figure that the grains are refined greatly for the effect of recrystallization in the first two passes. Then the grain size gets into a recrystallization and growth alternately occurred state during roughing rolling. Subsequently, the grain size reduces to a relatively small value during the intermediate rolling due to the decreasing temperature. After finishing rolling, the grains are refined again. This is mainly because of the reduced recrystallization grain size for the relatively low temperature and small reduction.

The grain size distributions in the section of the rod piece at different rolling stages are also showed in Fig. 7. It is obvious that the average grain size decreases with the proceeding of the rolling process. The reason is that recrystallization reduces the average grain size and the effect of grain growth on the average grain size decreases due to the decreasing temperature. In addition, it is found that the distribution of the grain size is inhomogeneous. The grain size is relatively large in the central part of the rolling piece, is relatively small near the surface, and is smallest around the corner of the rod piece. This is mainly because the size of the rod is large which induced the inhomogeneous temperature in the section of the rod, as shown in Fig. 4(a). The temperature in the central part of the rod piece is much higher than that near the surface, and the temperature is lowest around the corner. And the recrystallization grain size and effect of grain growth decrease with the
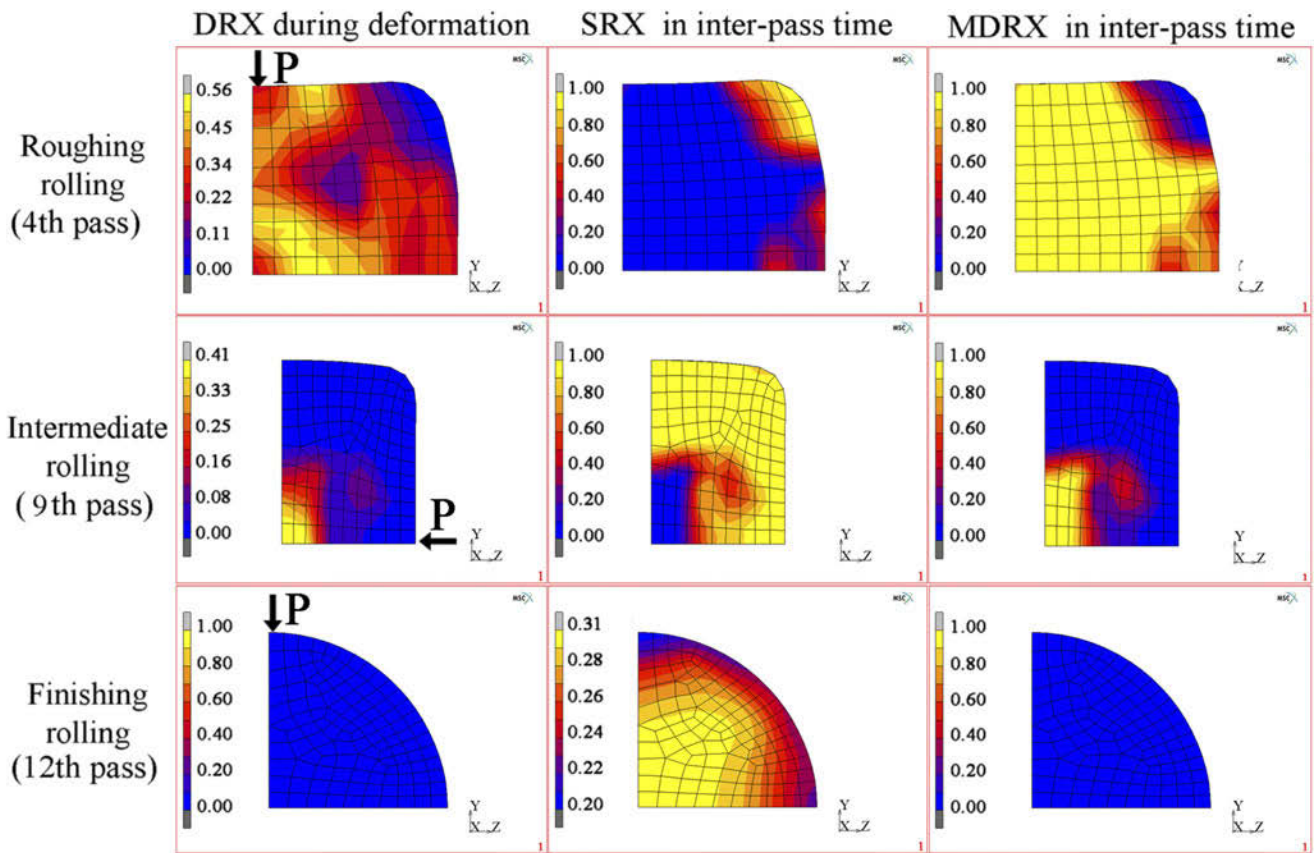
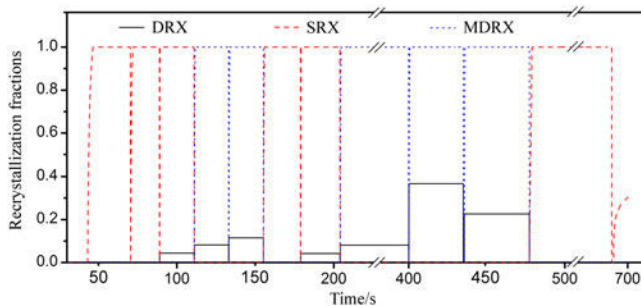FIG. 5. Distribution of recrystallization fraction during the rolling process.

FIG. 6. Evolution of recrystallization fractions at the center of the rolled piece.

FIG. 7. Evolution of the average grain size during the rolling process.

decreasing of temperature. So the distribution of the grain size is inhomogeneous.

3. Verification of simulation result

To verify the simulation result of the FEM, some samples are cut from the rod after rolling. And the optical microstructures at different positions of the sample are obtained as shown in Fig. 8. Because austenite has transformed into ferrite, pearlite, bainite, and martensite during the cooling process, the original austenite grain boundaries can be etched in martensite
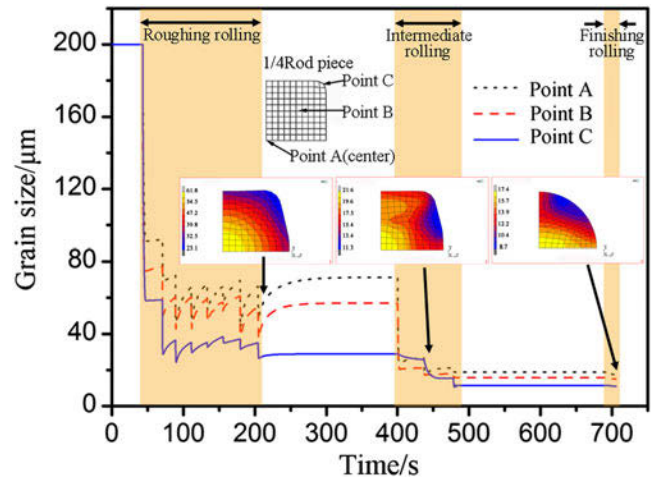
or bainite or described by netted ferrite. Generally, original austenite can be described clearly, and the measured values agree with the predicted ones, indicating that the work in this paper can provide guidance for designing optimal processing of large sized Nb–V microalloyed steel rods during TMCP.
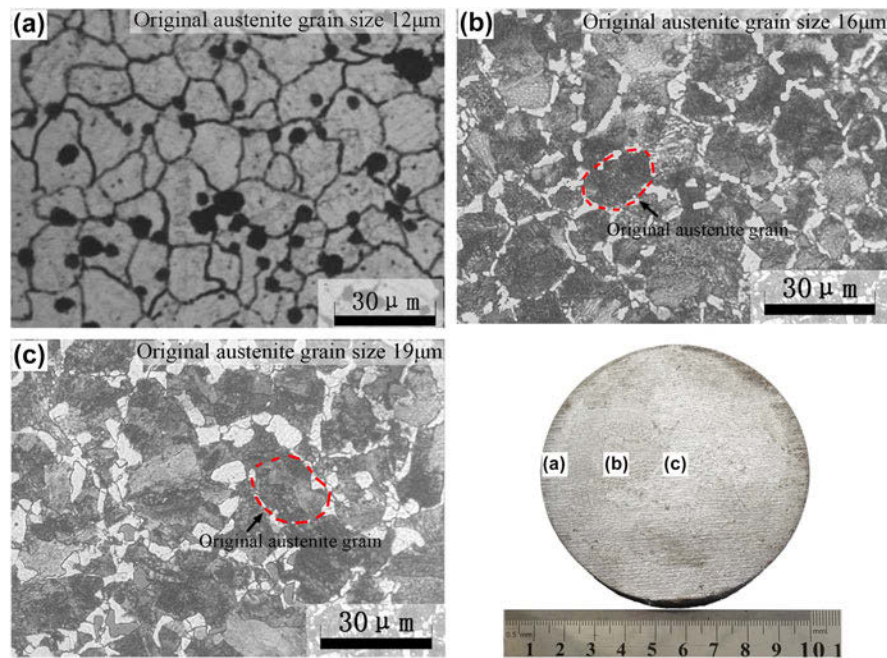
FIG. 8. Optical microstructure at different positions of the sample.

V. CONCLUSIONS

(1) A series of isothermal hot compression tests of Nb–V microalloyed nonquenched and tempered steel are carried out. Based on the obtained experimental data, the DRX, MDRX, and SRX models of the tested steel are developed.

(2) Using MSC.Marc software, a secondary development subroutine for the calculation of microstructure evolution is built. An FE model coupled with the microstructure evolution of large sized Nb–V microalloyed steel rods during TMCP is established.

(3) The recrystallization behavior and microstructure evolution during TMCP are simulated. And the simulated results agree well with the experimental ones, which illustrates that the recrystallization models of the tested steel and the FE model of large sized steel rods during TMCP are reliable. This research is helpful for designing optimal processing of large sized Nb–V microalloyed steel rods during TMCP.

ACKNOWLEDGMENTS

REFERENCES

1. Y. Luo, J.M. Peng, H.B. Wang, and X.C. Wu: Effect of tempering on microstructure and mechanical properties of a non-quenched bainitic steel. *Mater. Sci. Eng., A* **527**, 3427–3433 (2010).

2. S.D. Gu, L.W. Zhang, J.H. Ruan, P.Z. Zhou, and Y. Zhen: Constitutive modeling of dynamic recrystallization behavior and processing map of 38MnVS6 non-quenched steel. *J. Mater. Eng. Perform.* **23**, 1062–1068 (2014).

3. P.R. Spena and D. Firrao: Thermomechanical warm forging of Ti–V, Ti–Nb, and Ti–B microalloyed medium carbonsteels. *Mater. Sci. Eng., A* **560**, 208–215 (2013).

4. A. Kaynar, S. Gündüz, and M. Türkmen: Investigation on the behavior of medium carbon and vanadium microalloyed steels by hot forging test. *Mater. Des.* **51**, 819–825 (2013).

5. C. Sommitsch and W. Mitter: On modelling of dynamic recrystallisation of fcc materials with low stacking fault energy. *Acta Mater.* **54**, 357–375 (2006).

6. E.I. Poliak and J.J. Jonas: A one-parameter approach to determine the critical conditions for the initiation of dynamic recrystallization. *Acta Mater.* **44**, 127–136 (1996).

7. W.F. Shen, L.W. Zhang, C. Zhang, Y.F. Xu, and X.H. Shi: Constitutive analysis of dynamic recrystallization and flow behavior of a medium carbon Nb–V microalloyed steel. *J. Mater. Eng. Perform.* **25**, 2065–2073 (2016).

8. G. Kugler and R. Turk: Modeling the dynamic recrystallization under multi-stage hot deformation. *Acta Mater.* **52**, 4659–4668 (2004).

9. Y.C. Lin, Y-X. Liu, M-S. Chen, M-H. Huang, X. Ma, and Z-L. Long: Study of static recrystallization behavior in hot deformed Ni-based superalloy using cellular automaton model. *Mater. Des.* **99**, 107–114 (2016).

10. S.S. Zhang, M.Q. Li, Y.G. Liu, J. Luo, and T.Q. Liu: The growth behavior of austenite grain in the heating process of 300M steel. *Mater. Sci. Eng., A* **528**, 4967–4972 (2011).

11. L. Llanos, B. Pereda, B. Lopez, and J.M. Rodriguez-Ibabe: Hot deformation and static softening behavior of vanadium microalloyed high manganese austenitic steels. *Mater. Sci. Eng., A* **651**, 358–369 (2016).

12. R.D. Doherty, D.A. Hughes, F.J. Humphreys, J.J. Jonas, D. Juul Jensen, M.E. Kassner, W.E. King, T.R. McNelley,

H.J. McQueen, and A.D. Rollett: Current issues in recrystallization: A review. *Mater. Sci. Eng., A* **238**, 219–274 (1997).

13. C. Zhang, L.W. Zhang, W.F. Shen, C.R. Liu, Y.N. Xia, and R.Q. Li: Study on constitutive modeling and processing maps for hot deformation of medium carbon Cr–Ni–Mo alloyed steel. *Mater. Des.* **90**, 804–814 (2016).

14. H. Beladi, P. Cizek, and P.D. Hodgson: The mechanism of metadynamic softening in austenite after complete dynamic recrystallization. *Scr. Mater.* **62**, 191–194 (2010).

15. H. Beladi, P. Cizek, and P.D. Hodgson: New insight into the mechanism of metadynamic softening in austenite. *Acta Mater.* **59**, 1482–1492 (2011).

16. F. Chen, D.S. Sui, and Z.S. Cui: Static recrystallization of 30Cr2Ni4MoV ultra-super-critical rotor steel. *J. Mater. Eng. Perform.* **23**, 3034–3041 (2014).

17. Y.H. Liu, Y.Q. Ning, Z.K. Yao, Y.Z. Li, and J.L. Zhang: Dynamic recrystallization and microstructure evolution of a powder metallurgy nickel-based superalloy under hot working. *J. Mater. Res.* **31**, 2164–2172 (2016).

18. X.T. Li, M.T. Wang, and F.S. Du: A coupling thermal mechanical and microstructural FE model for hot strip continuous rolling process and verification. *Mater. Sci. Eng., A* **408**, 33–41 (2005).

19. F. Chen, F.C. Ren, J. Chen, Z.S. Cui, and H.G. Ou: Microstructural modeling and numerical simulation of multi-physical fields for martensitic stainless steel during hot forging process of turbine blade. *Int. J. Adv. Manuf. Technol.* **82**, 85–98 (2016).

20. C.X. Yue, L.W. Zhang, J.H. Ruan, and H.J. Gao: Modelling of recrystallization behavior and austenite grain size evolution during the hot rolling of GCr15 rod. *Appl. Math. Modell.* **34**, 2644–2653 (2010).

21. H. Jiang, L. Yang, J.X. Dong, M.C. Zhang, and Z.H. Yao: The recrystallization model and microstructure prediction of alloy 690 during hot deformation. *Mater. Des.* **104**, 162–173 (2016).

22. K.H. Jung, H.W. Lee, and Y.T. Im: Numerical prediction of austenite grain size in a bar rolling process using an evolution model based on a hot compression test. *Mater. Sci. Eng., A* **519**, 94–104 (2009).

23. A. Laasraoui and J.J. Jonas: Prediction of temperature distribution, flow stress and microstructure during the multipass hot rolling of steel plate and strip. *ISIJ Int.* **31**, 95–l05 (1991).

24. Q. Ma, Z.Q. Lin, and Z.Q. Yu: Prediction of deformation behavior and microstructure evolution in heavy forging by FEM. *Int. J. Adv. Manuf. Technol.* **40**, 253–260 (2009).

25. M. Wang, H. Yang, C. Zhang, and L.G. Guo: Microstructure evolution modeling of titanium alloy large ring in hot ring rolling. *Int. J. Adv. Manuf. Technol.* **66**, 1427–1437 (2013).

26. F. Yin, L. Hua, H.J. Mao, X.H. Han, D.S. Qian, and R. Zhang: Microstructural modeling and simulation for GCr15 steel during elevated temperature deformation. *Mater. Des.* **55**, 560–573 (2014).

27. X.G. Fan, H. Yang, and P.F. Gao: Through-process macro-micro finite element modeling of local loading forming of large-scale complex titanium alloy component for microstructure prediction. *J. Mater. Process. Technol.* **214**, 253–266 (2014).

28. H.Y. Zhang, S.H. Zhang, Z.X. Li, and M. Cheng: Hot die forging process optimization of superalloy IN718 turbine disc using processing map and finite element method. *Proc. Inst. Mech. Eng., Part B* **224**, 103–110 (2010).

29. J.H. Beynon and C.M. Sellars: Modelling microstructure and its effects during multipass hot rolling. *ISIJ Int.* **32**, 359–367 (1992).

30. J.J. Jonas, X. Quelennec, L. Jiang, and É. Martin: The Avrami kinetics of dynamic recrystallization. *Acta Mater.* **57**, 2748–2756 (2009).

31. A.M. Elwazri, E. Essadiqi, and S. Yue: Kinetics of metadynamic recrystallization in microalloyed hypereutectoid steels. *ISIJ Int.* **44**, 744–752 (2004).

32. Y.C. Lin, G. Liu, M.S. Chen, and J. Zhong: Prediction of static recrystallization in a multi-pass hot deformed low-alloy steel using artificial neural network. *J. Mater. Process. Technol.* **209**, 4611–4616 (2009).

33. D.Q. Dong, F. Chen, and Z.S. Cui: Modeling of austenite grain growth during austenitization in a low alloy steel. *J. Mater. Eng. Perform.* **25**, 152–164 (2016).

34. S.R. Wang and A.A. Tseng: Macro- and micro-modelling of hot rolling of steel coupled by a micro-constitutive relationship. *Mater. Des.* **16**(6), 315–336 (1995).

35. T. Siwechi: Modelling of microstructure evolution during recrystallization controlled rolling. *ISIJ Int.* **32**, 368–376 (1992).

36. S.Y. Yuan, L.W. Zhang, and S.L. Liao: Simulation of deformation and temperature in multi-pass continuous rolling by three-dimensional FEM. *J. Mater. Process. Technol.* **209**, 2760–2766 (2009).

37. S.L. Liao, L.W. Zhang, and S.Y. Yuan: Modeling and finite element analysis of rod and wire steel rolling process. *J. Univ. Sci. Technol. Beijing* **15**, 412–419 (2008).